Radiation Measurements 142 (2021) 106544

Contents lists available at ScienceDirect

Radiation Measurements

journal homepage: http://www.elsevier.com/locate/radmeas

Evaluation of physical retrospective dosimetry methods in a realistic accident scenario: Results of a field test

Michael Discher [a,b,*], Clemens Woda [b], Daniela Ekendahl [c], Carlos Rojas-Palma [d], Friedrich Steinhäusler [e]

[a] Paris-Lodron-University of Salzburg, Department of Geography and Geology, Salzburg, Austria
[b] Helmholtz Zentrum München, Institute of Radiation Medicine, Neuherberg, Germany
[c] National Radiation Protection Institute (SURO), Prague, Czech Republic
[d] Belgian Nuclear Research Center SCK CEN, Mol, Belgium
[e] Paris-Lodron-University of Salzburg, Department Chemistry and Physics of Materials, Salzburg, Austria

ARTICLE INFO

Keywords:
Retrospective dosimetry
Field test
Accident dosimetry
Radiological exposure device
Fortuitous materials

ABSTRACT

The radiological incident in Cochabamba (Bolivia, 2002), where members of the general public where exposed to an unshielded Ir-192 radiation source whilst traveling on a bus was replicated here in an attempt to asses and evaluate emerging retrospective dosimetry methodologies using objects of daily life, that are either carried on or close to the human body or can be found in the vicinity of an individual. For this purpose an accidental exposure was simulated under controlled conditions in a secured area and an unshielded radioactive source was placed in the cargo compartment of a bus resembling a Radiological Exposure Device (RED). Water canisters and anthropomorphic phantoms were placed at selected seats on the bus and equipped with personal objects (mobile phones, chip cards) that had reference dosimeters attached to them. At one seat position, additional salt dosimeters and dental ceramics in the phantom were also tested. Two types of 8 h exposures were conducted: one with a source activity similar to the one in Cochabamba (0.65 TBq) and one with a stronger source (1.5 TBq) in order to have more samples with absorbed doses above the detection limit of the different methods. For 43 out of 61 resistor and glass samples from mobile phones, measured doses agreed within error limits with reference doses, but for some materials more research is needed for a more reliable application. In 13 cases outliers with a significant dose over- or underestimation were observed, 10 of these could be identified by combining the results of at least three dose assays. The field test thus evaluated the potential and limitation of retrospective dosimetry using personal objects and demonstrated the importance of using a multi-dosimeter approach to increase robustness of the method.

1. Introduction

In 2002 a radiological incident occurred in Cochabamba, Bolivia, in which 55 passengers were exposed to ionizing radiation due to a malfunction of an industrial ^{192}Ir γ-radiography source, which was incidentally transported for repairs as cargo on a passenger bus. The IAEA reconstructed the incident with a field experiment using TLDs to estimate the personal dose of the bus passengers and workers who handled the source (IAEA, 2004). Estimates of the doses to the passengers on the bus, using personal dosimeters attached on water bottles, indicated dose values between 0.01 and 0.5 Gy, but up to 1.2 Gy (feet location) (IAEA, 2004).

In the past decade new physical methods for emergency dosimetry have emerged, such as optically stimulated luminescence (OSL), thermally stimulated luminescence (TL) and Electron paramagnetic resonance (EPR) of so-called fortuitous dosimeters, which can be applied to determine the absorbed dose. If no personal dosimeter is available, mobile phones or other ubiquitous personal belongings, which are carried on or close to the body, can be used as accident dosimeters. Research has been carried out by different groups on e.g. surface mount resistors and inductors on the circuit board of mobile phones (Lee et al., 2017; Bassinet et al., 2017; Ekendahl and Judas, 2012), integrated circuits (Mrozik et al., 2017b; Sholom and McKeever, 2016), display glass (Discher et al., 2020; Kim et al., 2019; Bassinet et al., 2014a; Discher and

* Corresponding author. Paris-Lodron-University of Salzburg, Department of Geography and Geology, Salzburg, Austria.
E-mail address: michael.discher@sbg.ac.at (M. Discher).

https://doi.org/10.1016/j.radmeas.2021.106544
Received 5 October 2020; Received in revised form 27 January 2021; Accepted 8 February 2021
Available online 13 February 2021

Woda, 2013), screen protectors (Bassinet and Le Bris, 2020), touchscreen glass (McKeever et al., 2017, 2019; Discher et al., 2016, Fattibene et al., 2014), protective glass on the back of modern smartphones (Sholom et al., 2020), chip cards (Kim et al., 2020; Woda et al., 2012a), dust on the toboacco leaves of cigarettes and other personal objects (Ademola et al., 2017; Bortolin et al., 2011), banknotes (Mrozik et al., 2017a; Sholom and McKeever, 2014) and dental ceramics (Ekendahl and Judas, 2017). Some overviews have been published (Bailiff et al., 2016; ICRU, 2019; Woda et al., 2009). So far, these investigations were only carried out under laboratory conditions (i.e. blind tests in an inter-laboratory comparison in the framework of EURADOS group (Bassinet et al., 2014b)).

Within the framework of the European Commission co-funded security research project CATO (CBRN **C**risis management, **A**rchitectures, **T**echnologies and **O**perational procedures), a field experiment with a similar bus was carried out, which simulates the Bolivian radiological incident and the dose reconstruction by the IAEA in the aftermath of the accident. In this field test, physical methods of retrospective dosimetry were tested and verified in a realistic irradiation scenario using mobile phones and chip cards as emergency dosimeters, attached to water canisters and anthropomorphic phantoms. The results were compared to measured dose values from dosimeters placed in the mobile phone, TLDs, OSLDs and readouts of electronic personal dosimeters (EPD) fixed close to the mobile phones. In addition, the experimental values were compared to results of radiation transport calculations using a Monte Carlo code, which simulated the irradiation scenario of the emergency dosimeters in the bus on a sufficiently detailed level.

2. Materials and methods

2.1. Experimental setup

The field test was carried out in the week of 02. – 05. June 2014 on the premises of the Schwarzenberg caserne in Salzburg, Austria. A military bus (Mercedes Benz INTEGRO) was parked between earth walls, with containers placed behind the bus for complementary shielding. 15 water canisters, as a substitute for the human torso, and four anthropomorphic phantoms (provided by SCK-CEN, SURO, ISS and IAEA) were placed on pre-selected seats and equipped with personal objects and dosimeters. In general, one mobile phone and chip card was attached on the front lower level of each water canister, whereas for three out of four phantoms several mobile phones were affixed at the belt level; these were used for an inter-comparison within the EURADOS network (Fig. 1, lower left panel; Woda et al. (in preparation)). A table of the used mobile phones and their seat position can be found in the supplemental data. For the water canisters closer to the source personal dosimeters were put in four positions: front top, front bottom, left, right. TLDs were provided by SCK-CEN and IAEA and OSLDs by Helmholtz Zentrum München (HMGU, now Mirion Technologies Inc.). For the phantoms, TLDs and OSLDs were positioned at three levels: chest, stomach and bottom (below mobile phones). For the phantom provided by SURO, additional TLDs and salt dosimeters from SURO were attached at selected positions.

The end of the guide tube for the ^{192}Ir source was mounted on a tripod in the luggage compartment of the bus (Fig. 1, upper right panel). Two sources are used in the experiment: a stronger (A = 1.5 TBq) and a weaker source (A = 0.6 TBq).

A seating plan of the bus with the position of the radiation source is shown in Fig. 2. The full details of the experimental setup of the field experiment are given in Rojas-Palma et al. (2020).

2.2. Chronology of the experiment

The first day of the field experiment (2nd of June) was used to evaluate the setup, see what doses at the different seat positions can be expected and whether simple dose rate estimations based on the inverse square law, that were calculated in the planning phase of the field test, were sufficiently adequate. For this purpose only water canisters were placed on the 17 seat positions inside the bus and equipped solely with electronic personal dosimeters for immediate readout and subsequent evaluation. Two test irradiations with duration of 30 min each were

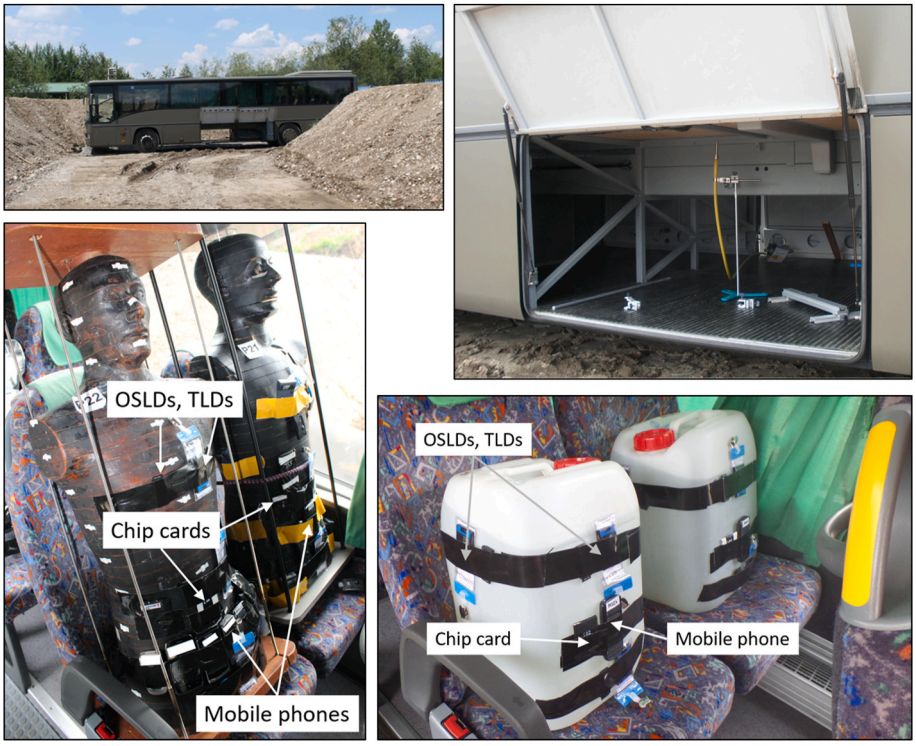

Fig. 1. View of the bus (top left), the end tip of the guide tube of the source in the compartment area (top right), anthropomorphic phantom (bottom left) and water canister (bottom right), equipped with mobile phones, chip cards (wrapped in black bag) and personal dosimeters.

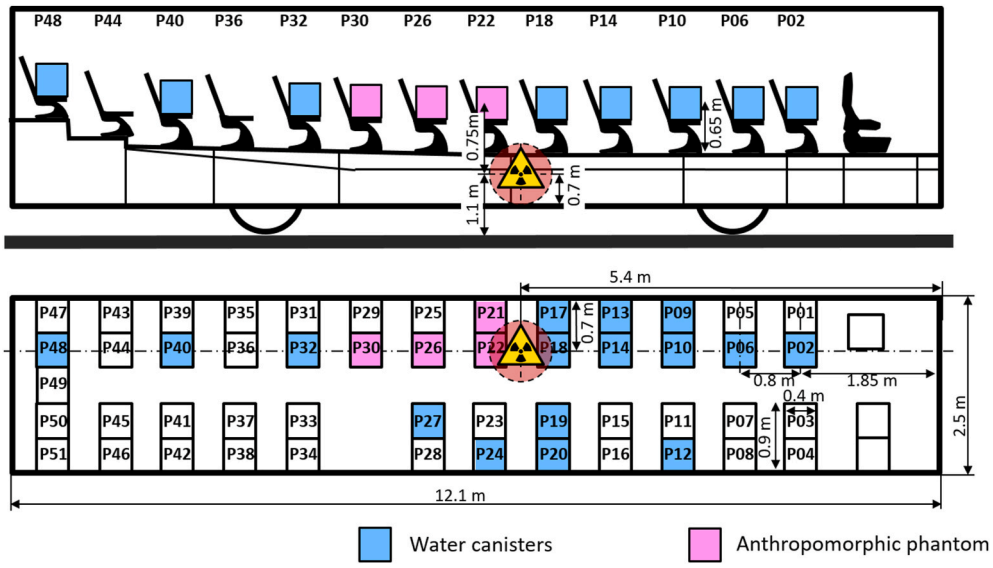

Fig. 2. Schematic view of the bus with positions of water canisters (in blue), anthropomorphic phantoms (in pink) and source (from Rojas-Palma et al. (2020)). (For interpretation of the references to color in this figure legend, the reader is referred to the Web version of this article.)

conducted. Additionally it was checked at which seat positions the detection limit of the emergency dosimeters was exceeded. After evaluation of the result, it was decided that the setup was adequate and could be used for the subsequent exposures.

On the following two days (3rd and 4th of June), two 8-h irradiations were performed with the strong source (A = 1.5 TBq). The four anthropomorphic phantoms replaced the water canisters at the selected seat positions and the personal objects were put, along with the TLDs and OSLDs, on the phantoms and water canisters.

On the last day of the field experiment a setup similar to the IAEA reconstruction of the Cochabamba accident (IAEA, 2004) was used. For this exercise all anthropomorphic phantoms and water canisters were equipped with a second set of personal items and the irradiation was carried out with the weaker (A = 0.6 TBq) source, again for 8 h.

2.3. Sample preparation

All personal items were equipped with one or several dosimeters in order to obtain reference dose values for each radiation sensitive component of the mobile phone or chip card.

LUXEL detectors (Landauer Inc.) consist of a polyester tape containing powder of carbon-doped aluminum oxide (Al_2O_3:C) and are thus of the same composition as the ceramic substrates of the electronic components on the circuit board. As such they are ideal reference dosimeter for evaluating the absorbed dose in both resistor and inductor substrates. The LUXEL detectors were fixed underneath the battery pack, to be as close to the circuit board and the target material (resistors and inductors) as possible (Fig. 3, left). In addition this provided sufficient shielding from day light and indoor lighting, which otherwise could bleach the dose information.

For the display glass material, three reference glasses were attached in equidistant positions on each screen of a mobile phone (Fig. 3, middle). The dimension of each glass piece is approximately 5 × 5 mm^2. Before the experiment the glasses were annealed in an oven to delete the intrinsic background signal, which would affect the dose readout.

For chip cards, two reference dosimeters were attached on each plastic card: Three BeO dosimeters beneath a black tape and one LUXEL detector. In addition, four chip modules, all from the same sample tape (production batch) provided by Infineon Technologies, were fixed on the plastic card (Fig. 3, right). 17 samples were small strips containing the chip, that had been cut from actual chip cards from different producers in Germany (health insurance, debit and credit cards). 34 samples were only plastic cards without chips, but of intact original size, that were then prepared with the four chip modules from Infineon and reference dosimeters. All chip cards were wrapped in black light-tight bags to consider light-shielding in wallets, which is where chip cards

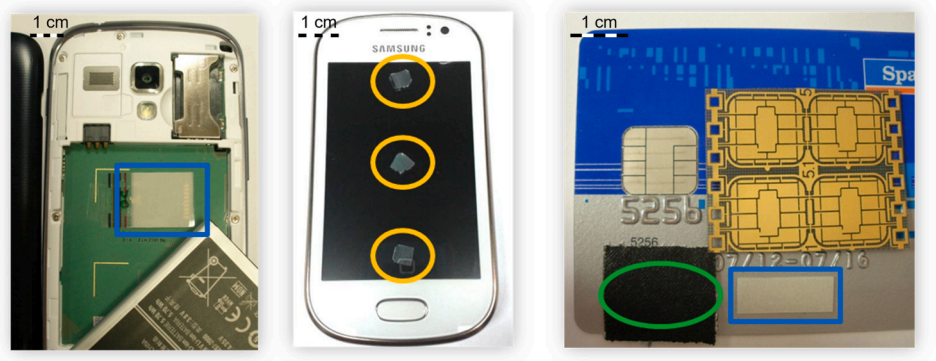

Fig. 3. Preparation of personal objects with reference dosimeters, prior to exposure in the bus. From left to right: LUXEL detectors (Al_2O_3:C) on the circuit board of mobile phones (blue); pre-treated reference glass samples on display glass (yellow); BeO dosimeters beneath black tape and LUXEL detectors on chip card (green and blue, respectively). (For interpretation of the references to color in this figure legend, the reader is referred to the Web version of this article.)

are normally placed.

After the end of the field experiment, the samples were brought back into the respective laboratories and further processed under subdues red light conditions.

Mobile phones were disassembled to extract the glass display and the circuit board using precision engineering tools to open the covering (i.e. Torx® screw drivers). Electronic components (resistors and inductors) were removed from the circuit board using a scalpel and cleaned for 15 min in acetone using an ultrasonic bath, in order to remove glue residue (Ademola and Woda, 2017; Fiedler and Woda, 2011). For most of the phones, three sizes of surface mount resistors could be found with dimensions (length x width): 0.5 mm × 0.3 mm (Code 0201), 1 mm × 0.5 mm (Code 0402) and 2 mm × 1.25 mm (Code 0805). For the phones irradiated with the strong source two measuring cups with resistors were prepared per phone for measurement with two different protocols (see section below), for the phones irradiated with the weaker source only one cup. To maximize sensitivity at least 20 resistors of type 0402 were placed on each cup, and, whenever available, two 0805 resistors (maximum amount per phone, when present) added. Only in a few cases not enough 0402 resistors could be found on the circuit board and in these cases, 0201 resistors were added. For display glass, all measurements were conducted on glass samples, etched in 40% HF, in order to reduce the intrinsic background dose signal (Discher et al., 2013).

Chips were punched out of the plastic cards and placed into the measuring cups with the transparent encapsulation facing upwards, towards the PM tube of the luminescence reader.

Almost all samples were measured between 10 and 36 days after exposure. Only inductors measured by TL were processed 72 days after exposure. Following the derivation in Aitken (1985) for anomalous fading, the middle of the irradiation time in the bus was taken as the reference point in time for calculating the fading time for all materials investigated. This approach is probably not entirely accurate for samples showing a mixture of thermal and athermal effects (e.g. chip cards) but is seen here as a reasonable approximation. Since storage times after exposure are much larger than the exposure time itself, any uncertainties introduced by considering different reference times for fading correction are around 2% or less and thus can be neglected in comparison to the uncertainties in the fading correction factors themselves (see below).

2.4. Measurement protocols and calibration

All measurements were conducted on Risø TL/OSL automated readers (DA15 and DA20), equipped with blue LEDs (470 ± 30 nm, 36 mW cm^{-2} and 20 mW cm^{-2}, respectively) for stimulation and a Thorn-EMI 9235 bialkali or an EMI 9235QB photomultiplier combined with a 7.5 mm U-340 Hoya filter (290–370 nm) for detection. The built-in $^{90}Sr/^{90}Y$ sources of the respective instruments were individually calibrated for each material. For LUXEL detectors, BeO dosimeters, display (reference) glasses, chip cards, resistors and inductors this was done using a Cs-137 gamma source at the Helmholz Zentrum München, traceable to the primary standard in Germany (Physikalisch Technische Bundesanstalt, PTB). Irradiations were done free in air with the materials sandwiched between two 3 mm thick PMMA plates, for charged particle equilibrium. All doses reported for these materials are thus dose to air that would be obtained under the same irradiation conditions. From Monte Carlo simulations of the calibration setup it can inferred that the dose to the material is within four percent of the dose to air.

2.4.1. LUXEL detectors

The LUXEL detectors were cut into three aliquots and each aliquot measured at room temperature using blue OSL for 300 s. OSL decay curves were integrated for the first 4 s and for 296–300 s for determination of signal and background respectively. Three dose calibration points were used and a straight line fitted to the dataset for converting the measured OSL signal into an absorbed dose. The choice of calibration doses was guided by the independent dose information available from the EPD and/or personal dosimeter readings on the phantoms or water canisters (Rojas-Palma et al., 2020). Average and the combination of the standard deviation of the three aliquot doses per dosimeter and the uncertainty of the calibration doses (3.5%) were used as reference dose. For the detectors placed in the phones, the relative standard deviation varied between 1 and 9% with a median of 2%.

2.4.2. BeO dosimeters

The BeO dosimeters were read out at 50 °C using blue stimulation at 1% optical power for 5 s, with a 5 s measurement interval inserted before and after optical stimulation, in order to define a background signal (total measurement time of 15 s, see also (Woda et al., 2012b). Samples were preheated at 160 °C for 10 s prior to OSL measurement. The OSL signal between 5 and 8 s and the dark count signal, including OSL afterglow, between 13 and 15 s, were integrated for determination of signal and background, respectively. After measurement the dosimeters were annealed at 650 °C for 5 min in a muffle furnace, re-inserted into the OSL reader, irradiated with a calibration dose of (1.00 ± 0.04) Gy and read out again. The absorbed dose was determined by direct comparison of the measured OSL signal with the calibration dose OSL signal. Similar to the LUXEL detectors, the average and the combination of the standard deviation of the three dosimeter doses per chip card and the uncertainty of the calibration doses were used as reference dose. The relative standard deviation of the doses of the three dosimeters per card varied between 0.2 and 12% with a median of 3%.

2.4.3. Electronic components

For resistor substrates, two measurement protocols, the “full mode” and “fast mode” protocol, optimized for either accuracy or speed of response and developed within the FP7 project MULTIBIODOSE, were applied (Bassinet et al., 2014b). For the “fast mode” protocol, measurements are conducted at room temperature without preheat, whereas for the “full mode” protocol, samples are preheated for 10 s at 120 °C and measurements are conducted at a sample’s temperature of 100 °C. For both protocol a short OSL readout of 30 s and a single calibration dose of 5 Gy was used. OSL decay curves were integrated between 1-6 s and 6–12 s for determination of signal and background intensity, respectively. Measured doses were corrected for signal fading using a universal fading curve for each protocol. Error of the dose measurement was assessed by combining the error of a single OSL measurement, the uncertainty of fading correction and the uncertainty of the calibration value of the built-in beta source. Further details will be reported elsewhere (Woda et al., in prep). Following the methodology of Currie (2004) in a simplified form, a detection limit (DL) and critical dose was calculated for every resistor sample according to $DL = \frac{3.3\,\sigma}{m \cdot f}$, where σ is the signal noise of an unexposed sample, m the slope of the calibration curve and f the fading factor. It was assumed that the critical dose is half of this value. For determining the signal noise σ, resistor samples with the OSL signal below the critical level were used and the standard deviation per channel of the last 10 s of the OSL decay curve calculated. σ for each sample was then set as $\sqrt{2n}$ times this standard deviation, where n is the number of channels used for signal integration and the factor 2 accounts for background subtraction. An average of these σ was calculated and used for all other resistor samples. Resistors read out with the full mode protocol were measured 10 and 21 days after exposure, resistors read out with the fast mode protocol, 35 days after exposure.

Inductors were read out using both TL (72 days after exposure) and OSL (36 days after exposure), but only for selected mobile phones exposed with the strong source. The OSL protocol was identical to the protocol used for resistors while the TL protocol was based on the recommendations given in Fiedler and Woda (2011): preheat of 10 s at 120 °C, TL up to 400 °C at 2 °C.s^{-1}, test dose normalization (0.15 Gy), three calibration dose points (1.5 Gy, 3.4 Gy, 5.1 Gy) and correction for dose overestimation by dividing the measured dose by a universal

correction factor of 1.33 ± 0.12 (derived from the data shown in Fig. 7 in Fiedler and Woda (2011)). The glow curve of preheated inductors has two peaks, which in the samples investigated here occurred at temperatures of ~170 °C and 250–260 °C, and the higher temperature TL peak was used for intensity determination and integrated between 200 °C and 300 °C. No correction for fading was attempted as this effect was estimated to be no more than 20% after storage times of two months (Fiedler and Woda (2011)).

2.4.4. Glass displays

Glass displays were measured 13–17 days after exposure using TL up to a maximum temperature of 450 °C (with thermal background subtraction). Prior to each TL measurement the sample was bleached for 500 s with blue LEDs of the luminescence reader in order to isolate the hard-to-bleach component of the TL signal. Three dose calibration points were used to convert the measured TL signal into an absorbed dose. The measurement protocol is called "pre-bleached with blue LEDs" (Discher and Woda, 2013). The measured dose is then corrected for signal fading (using a universal fading correction curve and the corresponding time period between irradiation and measurement) and the median background dose (Discher and Woda, 2013). To increase robustness, three aliquots were removed from the display glass plate of each mobile phone screen and measured separately. The average of the three measurements and the 95% confidence interval was used as the final dose estimate. The detection limit immediately after irradiation is mainly determined by the variability in the intrinsic background (zero-dose) signal and was estimated at 76 mGy (Discher et al., 2013). Since almost all of the glass samples were measured between 13 and 17 days after exposure and since the degree of signal fading changes less than 3% during that time period, a universal detection limit of around 130 mGy was calculated.

Reference glasses were measured in the same way as display glasses, only in the data analysis an intrinsic background dose was not subtracted as this had been removed by the preconditioning of the reference glasses. The relative error of the reference glass dose per sample, which comprises standard deviation of the three dose measurements per phone, fading correction and calibration uncertainty varied between 6 and 8%, with median of 7%.

2.4.5. Chip cards

Chip cards were read out 25–27 days after exposure using blue optical stimulation at room temperature with no preheat (Woda and Spöttl, 2009). A two-step readout protocol was applied, where in a first step a rapid screening protocol is used, involving a single calibration dose of (1 ± 0.04) Gy and an OSL readout time of 30 s. Subsequently, for those samples showing an accident signal above background a full readout protocol, involving several calibration doses, longer readout times and sensitivity correction procedures was applied. Details are given in the appendix. Compared to Woda and Spöttl (2009), the integration interval of the OSL signal in the rapid screening protocol was reduced to 5 s to avoid including noise and to minimize the effect of an increasing baseline, which was observed for chip cards irradiated with low doses. The reason for this increasing baseline is possibly the mechanism of (thermo-)optical release of electrons in the chip encapsulating epoxy and transfer into the OSL trap(s) of the filler material (silica) of the same epoxy, as described in Woda and Spöttl (2009). In the full protocol the integration interval was optimized for each sample individually but was never above 5 s. For fading correction, the fading function given in Woda and Spöttl (2009) was used. In addition, an individual fading correction factor was determined by irradiating the chip card with 1 Gy after the read out, storing it at room temperature in the dark for the same time duration as between the field exposure and first read out, measuring the corresponding OSL signal and comparing it with the calibration dose signal. Furthermore, for the chip modules from the sample tape a second fading correction factor was determined in the same way as described before but on previously unused ("fresh") modules.

For the chip modules from the sample tape, three chips were measured per plastic card and the average and standard deviation reported. For the chips from the card themselves, the error of a single dose measurement was determined from the error of a single OSL measurement (in the same way as for resistors), the error of the test dose measurement (where applicable) and the uncertainty of the individual calibration curve by standard error propagation.

2.4.6. Household salt

Salt samples were measured using CW-OSL technique. The samples in form of a few salt grains were mounted on stainless steel cups. First, they were preheated at 200 °C for 10 s. The OSL signals were read with power of blue light source of 20 mW cm^{-2} for 20 s at 120 °C. Dose was reconstructed using SAR protocol (see details in Ekendahl et al., 2016). For fading correction, a universal correction curve was applied, which had been determined in a previous study (Ekendahl and Judas, 2011). In order to increase robustness and prove reproducibility, five aliquots were used for each position. The average dose in NaCl and standard deviation are reported.

2.4.7. Dental ceramics

Small samples of fluorapatite glass-ceramic were measured both using OSL and TL signal (Ekendahl et al., 2013). As for OSL signal measurement, the samples were preheated at 150 °C for 10 s, which was followed by CW-OSL reading using blue light of 20 mW cm^{-2} power for 60 s at room temperature. Subsequently, the TL signals were read during heating at rate of 5 °C.s^{-1} up to 450 °C. The peak at ~280 °C, which was resistant to optical bleaching, was employed.

Calibration dose of 3 Gy was used. For fading correction, a universal correction curve was applied, which had been determined in a previous study (Ekendahl et al., 2013). Eight samples were used in the experiment in order to observe the dose dependence of sample position in the teeth inside the head of the phantom. Doses are reported in terms of dose in ceramic.

2.5. Monte Carlo simulations

As a first step to verify the experimental results, radiation transport calculations were performed with the Monte Carlo code MCNP5 (MCNPX-Team, 2003) for simulation of the dose to air and to the glass display of the mobile phone. The geometry of the experiment, the bus and the mobile phones as dosimeters were integrated in detail into the simulation. Earth wall, ground, containers and bus were approximated by simplified geometries. Dimensions were taken from measurements and technical drawings. The material specifications were adopted from a standard literature source for radiation transport simulations (Williams et al., 2006).

In Fig. 4 a the geometry of the environment and in Fig. 4 b the bus interior are shown which are used for the simulations. The earthen walls and the containers were used for shielding in the field experiment. The water canisters, which were placed on selected seat positions, can be seen in the interior view of the bus. Small air cells were integrated into the simulation in front of the water canisters to detect the absorbed doses in air on each seat position. Additionally a realistic, detailed model of a mobile phone was included to calculate the absorbed dose in the glass material of the display (Discher et al., 2015, Discher et al., in prep.).

The absorbed dose in the corresponding material was calculated with the track length estimator tally (F6 tally with unit Gy/source particle) and converted into absorbed dose (unit Gy) using the decay corrected activity of the source, the exposure time and the emission probability per decay (also called photon yield).

In the simulation the iridium source was integrated as an isotropic point source in the luggage compartment of the bus. The simplified form of the source is justified by its small dimensions, with the radioactive capsule having a diameter of only 2 mm, which is negligible compared to the distance even of the closest detectors (>1 m). The photon energy

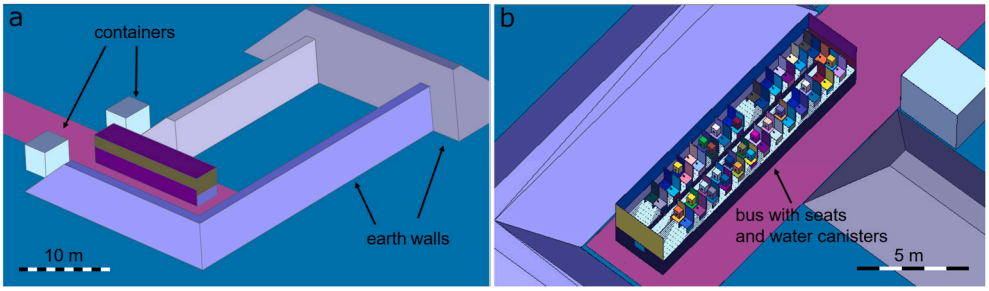

Fig. 4. a–b: Geometry of the environment and the bus interior used in the simulation.

spectrum of the Ir-192 source was taken from the tabulated gamma emission (Browne, 2003). In the simulation, the gamma source consists of discrete histograms from integrated energy and probabilities.

Next to the absorbed dose in glass, the photon energy spectrum in air at the different sample positions was also calculated, for discrete energy intervals E_i with width ΔE_i. Although doses to other target materials could not (yet) be considered in these preliminary Monte Carlo simulations, the energy spectra nevertheless were used to estimate the impact of the energy dependence of the different reference dosimeters to the dose absorbed in these materials. For this, the ratio R of absorbed dose in the dosimeter to air kerma was calculated as:

$$R = \sum_i R(E_i) \cdot \overline{\phi}(E_i) \cdot \Delta E_i$$

where E_i is the center energy of the ith energy bin, $R(E_i)$ the dose ratio at E_i, $\overline{\phi}(E_i)$ the relative photon fluence (in air) within the ith energy bin and ΔE_i the bin width (see also Ulanowski et al. (2021)). $R(E_i)$ was approximated by the ratio of calculated mass-energy absorption coefficients in the dosimeter and air:

$$R(E_i) = \frac{\left(\frac{\mu_{en}}{\rho}\right)_{Dosimeter}}{\left(\frac{\mu_{en}}{\rho}\right)_{Air}}(E_i)$$

This simplified approach assumes kerma conditions and does not consider angular dependencies but is seen here as a sufficient approximation for discussion of the experimental data. Mass-energy absorption coefficients for LUXEL detectors (Al_2O_3), BeO dosimeters and air were calculated using data obtained from the National Institute of Standards and Technology (NIST) database (Hubbell and Seltzer, 2004) and the weight fractions of the different elements (Al, O, Be) in the compound media. This approach has been shown to produce results that compare well with experimental data obtained for the two types of detectors in reference conditions (Gasparian et al., 2012; Sommer et al., 2007).

3. Results and discussions

3.1. Reference dosimeters on personal objects

The results of the individual personal dosimeter readings (TLDs and OSLDs mounted on water canisters and phantoms) are published and discussed in detail in Rojas-Palma et al. (2020). The personal dosimeter

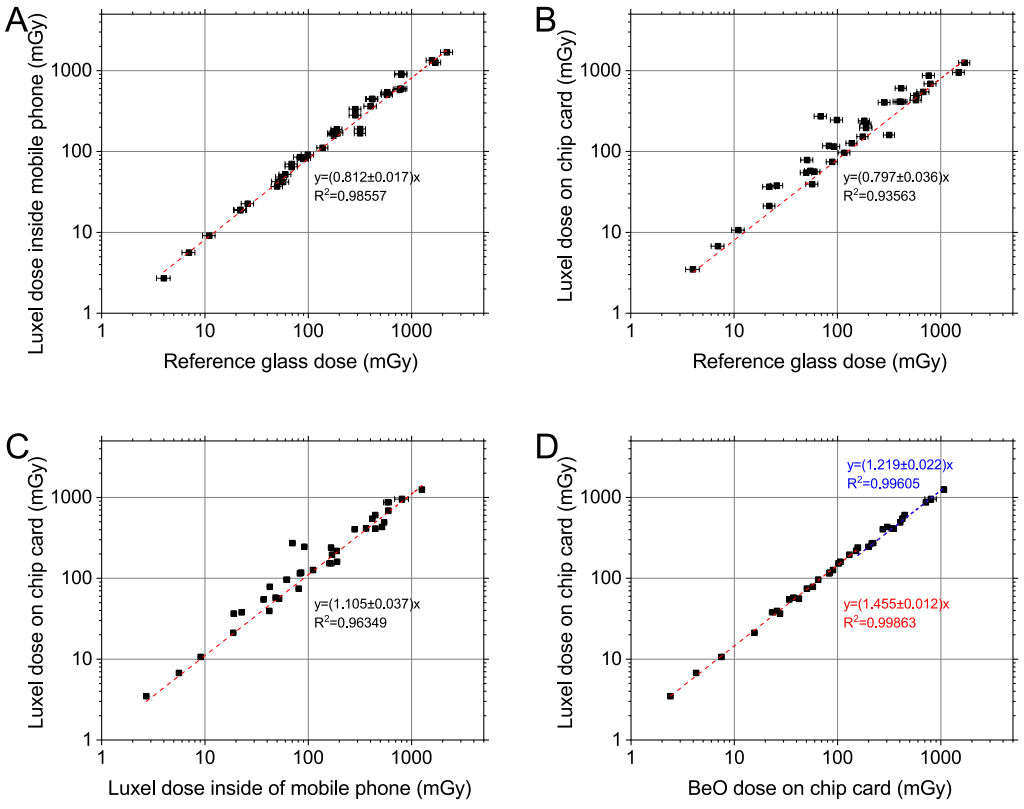

Fig. 5. a–d: Comparison of absorbed doses measured by different reference dosimeters on the personal objects. From top left to bottom right: A) Comparison of absorbed dose in LUXEL detectors behind the circuit boards of the mobile phones with the absorbed dose in reference glass dosimeters on the display glass. B) Comparison of absorbed dose in LUXEL detectors on the chip cards with absorbed dose in reference glass dosimeters. C) Comparison of absorbed dose in LUXEL detectors on the chip cards with absorbed dose in LUXEL detectors behind the circuit boards of the mobile phones. D) Comparison of absorbed dose in LUXEL detectors on the chip cards with absorbed dose in BeO dosimeters on the same cards.

readings served to map the dose distribution throughout the bus and were used to visualize the heterogeneity of exposure and shielding effects for seat positions close to the source. In this work focus is on the reference dosimeters which were placed on and in the personal objects and the results are compared and discussed in this subsection. The comparison of absorbed doses by the different reference dosimeters illustrates dose gradients within mobile phones and the possible effect of scattered radiation. Fig. 5 a-d show the comparison of the absorbed doses measured by the different reference dosimeters on and in the mobile phone and on the chip cards.

As expected there is a strong correlation between the doses recorded by the different reference dosimeters, with a lower degree of scatter observed for the data from reference dosimeters placed on the same personal item (Fig. 5 a and d) as compared to the data from reference dosimeters on two different items (reference dose on chip card with reference dose in glass of mobile phone or with dose in aluminum oxide inside mobile phone, Fig. 5 b and c). The latter is most likely due to the fact that mobile phones and chip cards were not always placed sufficiently close to each other on the water canisters/phantoms, which, depending on the seat position and orientation towards the source, resulted in differences in the degree of shielding of the two items.

The situation is somewhat different for the two different types of dosimeters on the chip cards (LUXEL detectors (Al_2O_3) and BeO chips, Fig. 5 d) and requires closer inspection. Overall there is an excellent correlation between the two dosimeter types, which is expected as they are placed very close to each other on the same item (Fig. 3, right), so that there are no significant differences in positioning, gradients and shielding. On the other hand, the data fall into two groups with different slope of the linear fit. For the higher dose region, average doses in Al_2O_3 are roughly 20% higher than in BeO, for the lower dose region the difference amounts to almost 50%. Lower doses occur for the more distant seating positions and for cards closer to the source but with stronger shielding. In both cases a higher degree of scattered radiation is expected than for the less, or unshielded dosimeters closer to the source. As BeO has a slight underresponse (20%) for low (<100 keV) photon energies, whereas LUXEL detectors tend to overestimate the dose with respect to air kerma up to a factor of 3–4 for low energies (Gasparian et al., 2012), the higher slope for the lower dose data points in Fig. 5 d would be qualitatively explainable by such an effect. For a more quantitative estimation, the approach described in section 2.5 is used. The results of the Monte Carlo simulations will be presented in section 3.5, here the photon spectra in air in front of the phantom on seat number 22 and in front of the water canister on seat number 48 are used as two examples of positions with minor (22) and maximum (48) amount of scattered radiation. Combining the simulated spectra with the energy dependence of the two types of dosimeters, the latter calculated from the mass-energy absorption coefficients, results in estimates of the ratio of absorbed doses in Al_2O_3 to BeO of 1.06 and 1.20 for seat positions 22 and 48, respectively. The radiation transport calculations thus do support the increase of the slope in Fig. 5 d with decreasing dose (increasing amount of scattered radiation), the experimental effect however is a factor of two higher than the calculated one. The reason for this discrepancy is at present not understood. The precision of the individual dose measurement in Fig. 5 d for both types of detectors is on average 3% or better. Calibration was done using the same gamma source and setup, therefore uncertainty in the calibration should not have a major impact. Further systematic comparisons of the two dosimeter types and protocols in reference conditions and a full modelling of the field test setup for the reference dosimeters is needed. Despite the discrepancies, the data serve as a first indication that a softening of the photon spectrum is probably present for certain detector positions but that at the same time the absorbed doses in the detectors do not deviate by more than 20–50% from the respective air kerma values. This should by and large also apply to the radiation sensitive components of the personal items. Further support will be given the Monte-Carlo simulations of the dose in display glass in section 3.5.

The on average 20% lower dose recorded by the LUXEL detectors in the phone compared to the reference glasses on the phone, that can be seen in Fig. 5 a, is unlikely to be caused by effects of energy dependence, since the over-response of display glass and LUXEL detectors is very similar (Gasparian et al., 2012; Discher et al., 2015). A more probable reason are dose gradients within the phone.

3.2. Mobile phones

3.2.1. Electronic components

The results of the dose assessment using resistors of the circuit board are shown in Fig. 6 a-b. Reference values are the absorbed doses in the LUXEL detectors, placed beneath the battery. Measurements were conducted between eight and 20 days after the exposure. For both exposure days with the 0.65 TBq (right panel) and 1.5 TBq (left panel) source a good agreement between reference dose values and measured doses in the resistor substrates for doses above 30 mGy and for the “full mode” protocol (“with preheat”) is seen. Excluding the two data points in Fig. 6 a with the lowest reference dose, a weighted linear fit through origin yields slopes of 0.94 ± 0.06 ($R^2 = 0.945$) and 0.90 ± 0.06 ($R^2 = 0.943$), for the datasets in Fig. 6 a and b, respectively. For the exposure day with the stronger source, a second set of resistors per mobile phone was extracted and measured with the “fast mode” protocol (without preheat). Although the uncertainty of an individual measurement using this protocol is higher, due to a larger degree of variability in fading rates, overall the level of agreement between measured and reference dose is similar to the measurements with the full mode protocol. Again omitting the two lowest dose data points, the slope of the weighted linear regression is 0.87 ± 0.11, which agrees within unity within the uncertainty. Both approaches thus seem to perform on an equally acceptable level, in terms of degree of scatter of individual measurements and overall agreement with the reference doses, an observation which is in agreement with the results of a previous study (Bassinet et al., 2014b).

The degree of scatter of the data points around the 1:1 line seems to be somewhat larger than expected form the individual uncertainty assessment, however it should be kept in mind that the error bars plotted indicate the 1 σ uncertainty range. More quantitatively, the difference between measured and reference dose is outside the 95% confidence interval (statistically significant) for eight samples while for 37 samples measured and reference dose agree within error limits. Thus in the majority of cases the uncertainty assessment seems to account for the observed scatter. The median relative error is 16 and 34% for the full and fast mode protocol, respectively, and the difference to the reference dose never exceeded 3 σ. The level of accuracy achieved is therefore sufficient for triage and also for dose assessment within the context of emergency dosimetry.

The median detection limit and critical dose were 72 and 36 mGy for the fast mode protocol and 52 and 26 mGy for the full mode protocol. Thus one would expect no doses to be detectable below around 30 mGy and indeed for e.g. the irradiations with the 0.65 TBq source, two phone samples with reference doses below 10 mGy gave doses indistinguishable from zero within uncertainty (only one is shown in Fig. 6 b, as the other sample gave a negative dose). On the other hand, there were also phone samples for both irradiation days which received doses below the respective critical doses and nevertheless doses were measured with the extracted resistors that overestimate the reference dose by a factor of more than two. The reasons for the latter observation are at present not clear. Since the energy dependence of resistors and LUXEL detectors are similar (although not necessarily identical), differences in absorbed doses due to softening of the photon spectrum in the low dose region (increased scattered radiation) should be less than for the LUXEL detectors and BeO dosimeters on the chip cards, i.e. less than 20–50% (see previous section). This is not sufficient to explain the overestimation. Another possibility is the existence of a zero dose signal in OSL of resistor substrates, similar to TL of glass and SMDs, which however has not been reported in the literature so far. It should be noted that

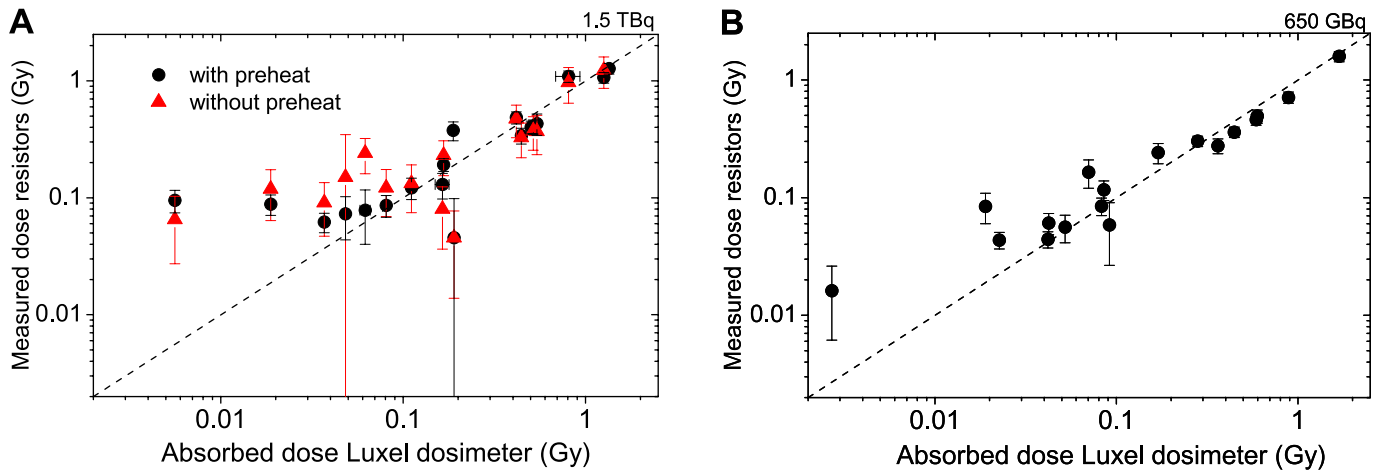

Fig. 6. a–b: Results of dose assessment using resistors from the mobile phone. For samples used during the exposure day with the 1.5 TBq source (A), two measurement protocols were applied. One mobile phone was accidentally irradiated for two subsequent days, the first day with the strong and the second day with the weak source. This explains the highest dose point in the right hand panel (B). The dashed lines represent the 1:1 correspondence.

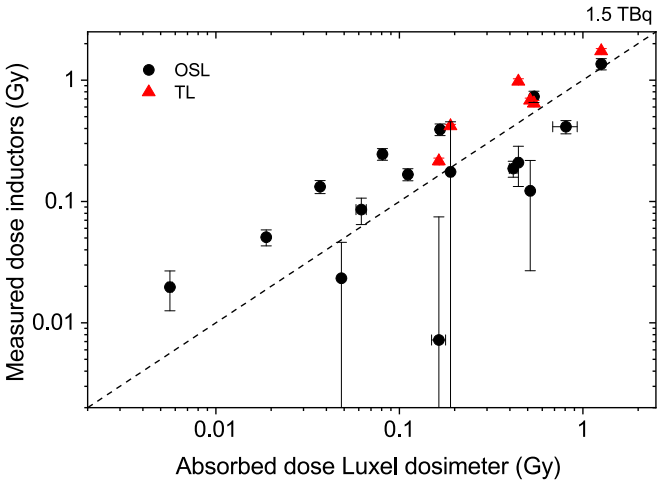

Fig. 7. Results of dose assessment using inductors extracted from the mobile phone. For measurements with OSL the fading factor derived from OSL measurements on resistors was used, whereas no fading correction was done for measurements with TL.

although the reasons for the discrepancy in the low dose region are not (yet) understood, the overestimation does not constitute a major problem for emergency dosimetry as the measured doses are still all on the order of 100 mGy or less.

For dose assessment using inductors, measured with both OSL and TL, the results are far less encouraging than the ones from resistors (Fig. 7). Doses measured by OSL fall into three groups: those with a significant higher fading rate than resistors, underestimating the reference dose, those with a similar fading rate as resistors, in agreement with the reference dose and those with a significant lower fading rate than resistors, which overestimate the reference dose. Obviously the ceramic body of inductors is less standardized and homogeneous than the one from resistors and a universal fading correction not applicable. Currently it is not known how to identify the fading category in which the samples fall into.

Doses measured by TL generally overestimate the reference doses, between 30% and up to a factor of two. Since no correction for fading was attempted in the case of TL, the overestimation cannot be the result of the application of an incorrect fading factor. Although inductors have an undoubtable potential for emergency dosimetry with the advantage of a general higher sensitivity and thus lower detection limit than resistors, more research is needed before this material can be established as a reliable dose reconstruction tool.

3.2.2. *Display glass*

The results for the dose assessment using display glass are shown in Fig. 8 a and b. A direct comparison between the results of the display glass and the results of the reference glass is carried out. The left panel shows the results of the irradiation using the 1.5 TBq Ir-192 source and the right panel the results using the 0.65 TBq source. In both graphs, the measured dose values are close to the bisector line, which is shown as dashed lines in the two diagrams, for the majority of samples. The detection limit of 130 mGy is also specified with a blue horizontal line. If the best estimate of the absorbed dose is below this detection limit of the method direct statement cannot be made within the 95% confidence interval whether the sample has been irradiated or not. However, in such a case the result can be used to estimate the upper limit of a possible dose. For the 27 samples for which doses above detection limit were measured, 17 agreed within the 95% confidence interval with the reference glass doses. Two samples at positions P32 and P40 marked in Fig. 8 a significantly overestimated the reference doses, one sample significantly underestimated the reference dose. Seven outliers with significant dose overestimation can be observed in Fig. 8 b.

A possible reason for the observed dose underestimation in one sample is an exceptionally high fading rate, which is not considered in the uncertainty (variability) of the applied universal fading correction factor. In turn, the reason for the significant dose overestimation in the other nine outliers is most likely found in an unaccounted exceptionally high intrinsic background signal. Indeed, a detailed examination of the TL measurements for these samples shows the presence of a very intense intrinsic zero dose signal in the high temperature range of TL glow curve. This signal is detected for all three aliquots of a display sample. The overestimation of the dose can be explained with this background signal. However, this observation is not expected because etching the glass samples significantly reduces the intrinsic zero dose signal (examined in Discher et al. (2013)). This leads to the assumption that in the investigation in Discher et al. (2013), the number of analyzed samples was not exhaustive and the full extent of the distribution of the zero dose signal could not be assessed with the 28 samples analyzed in the study. Therefore, it would be useful to have an additional method for identification of such outliers.

The unused information of the high-temperature range of the TL signal can be used for quality assurance to see if the converted value of the zero dose signal is within the distribution of previously analyzed samples. The corresponding zero dose for the integration range between

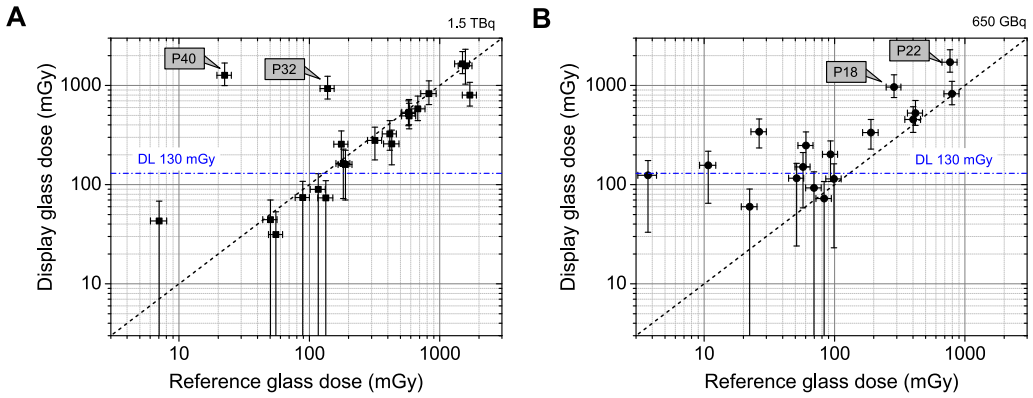

Fig. 8. a–b: Results of dose assessment using glass display from mobile phones.

300 and 450 °C is calculated from the remaining zero dose signal after the etching process. Similarly to the results in Discher et al. (2013), the distribution of the background dose for the high temperature range of the investigated etched glass samples can be described as a log-normal distribution. With a specified threshold of the background dose, the measurement results can be evaluated according to the selected p-quantile. With this new method, four out of the nine outliers with dose overestimation could be flagged (p-quantile: 0.950). The investigation shows that sample readouts can be evaluated with this new approach and the number of outliers reduced using a simple additional analysis in the same readout method. A further step in outlier identification would be the combination with further dose measurement methods and simulations. This will be described in section 3.6.

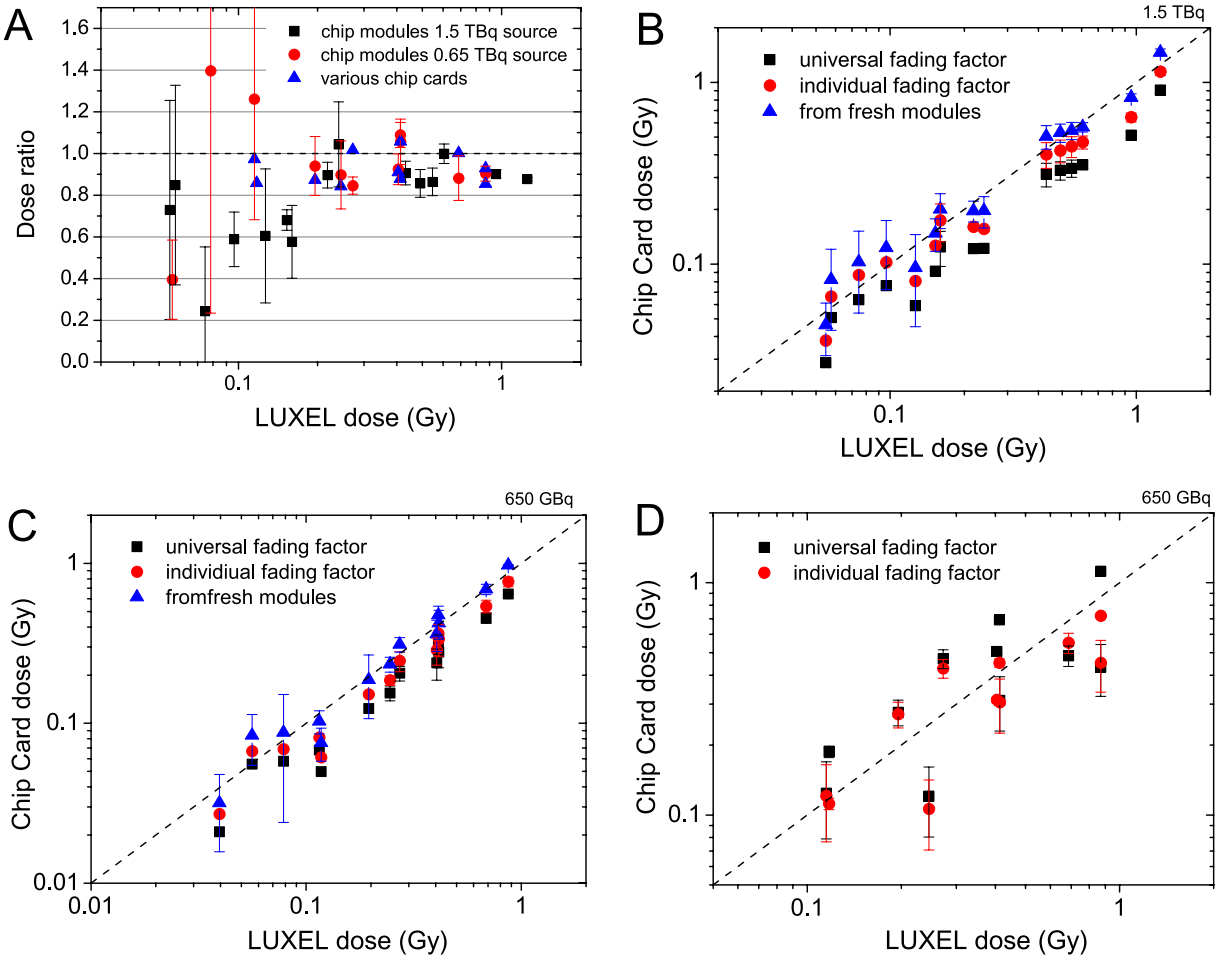

Fig. 9. a–d: Results of dose assessment using chip cards: Dose ratio using the fast screening and full protocol for all three sets of chip cards and exposure days (A). Dose assessment using the same production batch (Infineon) for the exposure day with the 1.5 TBq source (B) and the 0.65 TBq source (C). Plotted values are dose averages of three chip modules per datum point. For the sake of clarity error bars were omitted for the "universal" and "individual fading factor" data points in the lower dose range. Results of dose assessment using arbitrary chip cards for the exposure day with the 0.65 TBq source (D).

3.3. Chip cards

The comparison of the fast screening and full protocol for chip cards is given in Fig. 9 a, the results of the dose assessment using homogeneous chip cards from the same production batch for two irradiation days in Fig. 9 b and c and the results for the arbitrary chip cards from different producers in Fig. 9 d. Results for the dose ratio of fast to full protocol are similar to the ones obtained in the lab test preceding the field test. Below around 200 mGy, doses measured with the fast screening approach amount to about 60% of the doses measured with the full protocol, with a large variation, while for higher doses this percentage varies between 80 and 100%. This implies that the performance of the fast screening protocol seems to be adequate also under the field conditions for a first quick rough dose estimate. The results in the other panels shown in Fig. 9 are all the ones obtained with the full protocol. For the homogeneous chip cards from the same production batch there is a clear strong correlation between the measured dose in the chip encapsulation and the absorbed dose in the reference dosimeter, however, when using the universal fading correction factor, doses are underestimated by approximately 35%. This applies to both days of exposure with the 0.65 TBq and 1.5 TBq source (Fig. 9 b and c). If the individual fading factors are applied, measured doses come within 20% of the reference dose values and with a fading factor inferred from fresh, previously unexposed modules excellent agreement is observed over the entire dose range. Obviously, the degree of fading for this production batch differs from the one used for establishing the universal fading correction curve (Woda and Spöttl, 2009). Doses below 40 mGy resulted in OSL signals measured with the rapid screening method that were below the critical level and these modules were then not further processed.

For the arbitrary chip cards from different producers, the situation is more complex/less homogeneous (Fig. 9 d). These cards were exposed on the last day of the field experiment using the weaker (0.65 TBq) source. As no reference dosimeters were available to be placed on the cards, the absorbed dose in the LUXEL detectors on adjacent plastic cards with the Infineon chip modules were used as reference values. The chips on the cards had variable sizes of encapsulation, especially the health insurance cards from Germany had chips and encapsulations of approximately half the size of the modules. Consequently, the critical dose was around 100 mGy (for measurements at 26 days after exposure). For the 18 exposed cards, seven received doses below the individual critical dose, leaving 11 analyzable results. Compared to the chip card modules, a much larger degree of scatter of the data points in Fig. 9 d is observed, although there is still a clear correlation between measured and reference dose. When applying the individual fading factor instead of the universal one, there is a change in dose value around 40% for four samples, yielding a somewhat better agreement with the 1:1 line in the figure but for the majority of chip card samples there is little (~10%) to no change. This means that a variability in fading factor between the different types of chip cards is not the only reason for the observed scatter of data points. A second one is an issue of a higher systematic uncertainty in the reference dose, since the reference dosimeters were not on the same card and, depending on closeness to the source and shielding effects, this can lead to additional deviation between reference and measured dose. Calculating the weighted average and standard deviation of the ratio of measured to reference dose gives values of 1.26 ± 0.22 and 0.83 ± 0.10, for the datasets with universal and individual fading factor, respectively, which both agree with unity within the respective uncertainty. Despite the issues of reference dosimetry and variability in fading rates the field test could thus still demonstrate the potential of chip cards for emergency dosimetry in a realistic accident scenario, with the advantage of a fast, simple sample preparation (2–3 min) on an item of low replacement costs. More research into fading correction or the development of fading free protocols would however be advantageous.

3.4. Household salt and dental ceramics

All of results were obtained from the first day of measurement with the strong source with activity of 1.5 TBq. The phantom was placed near to the source, on the seat number 21. Salt tubes together with TLDs (personal dosimeters with four LiF:Mg,Cu,P detectors) above tubes were placed in two positions on phantom near to typical position of pockets on trousers. Additional TLDs were placed in position of chest and in front of the phantom. Eight samples with dental ceramics were placed into the phantom, in the position of teeth. The reason of using TLDs was as comparing results with results from salt tubes as showing the strong left-right gradient of dose distribution. The dose from salt tubes in chest and from dental ceramics in comparison with the dose from the bottom of phantom shows also strong top-bottom gradient of dose distribution. The results from dental ceramics from different part of teeth show small gradient of dose distribution.

The results from salt tubes and TLDs are given in Table 1. From the results of TLDs reported in terms of personal dose equivalent $H_p(10)$, a strong dose gradient is observed. The TLD values are lower than results from adjacent salt tubes. One of the reasons may be different energy response of salt and TLD based on LiF:Mg,Cu,P. Salt is not a tissue equivalent material and tends to overestimate dose for lower photon energies (<250 keV) (Ekendahl et al., 2016). In addition, the positions of TLD sensitive part and salt tubes were close but not identical. A comparison of $H_p(10)$ and dose in NaCl can be done via dose to air leading to the relationship $H_p(10) = h_p(10) \cdot D_{NaCl} \cdot (\mu_{en}/\rho)_{air}/(\mu_{en}/\rho)_{NaCl}$. It requires a specific conversion coefficient $h_p(10)$ for the applied conditions of irradiation (gamma spectrum, angle of irradiation and position of the dosimeter on the phantom). Conversion coefficients are available for mono-energetic photons and for common simplified geometries of irradiation. However, using the existing data (ICRP, 1997; Zankl, 1999) and $(\mu_{en}/\rho)_{air}/(\mu_{en}/\rho)_{NaCl}$ values for average energy of ^{192}Ir and lateral irradiation (when the dosimeter is irradiated similarly) it can be derived that the ratio $H_p(10)/D_{NaCl}$ should be between 0.4 and 0.9, which is in correspondence with the results obtained.

The results from dental ceramics are shown in Table 2. A small variation of dose relative to position of dental ceramics is visible.

3.5. Results of Monte Carlo calculations

In Fig. 10 a the results of the simulation are shown for the stronger source (1.5 TBq). The absorbed dose in the glass material of the simulated mobile phone is compared to the values of the reference glasses in the experiment. A good correlation between the values can be seen. Additionally, the photon spectra at three selected seat positions (Pos. 22, 30 and 48) are shown (see Fig. 10 b-d). With increasing distance and shielding from the source, the amount of unscattered radiation is reduced and an overall softening of the gamma spectrum can be observed. This is more pronounced for glass as compared to air, due to the stronger absorption of lower energy photons by the glass display (Discher et al., 2014, 2015; Bassinet et al., 2014a). The cumulative distribution function on the other hand shows that even for the most distant seat position, the contribution of photons with energies lower than 100 keV to the total dose in air, the energy range in which the overresponse of glass and the other radiation sensitive materials investigated is most pronounced, is on the order of only 10%. This implies

Table 1
Dose in NaCl from small tubes and Hp(10) values from TLDs.

Position	Salt [mGy]	TLD [mSv]
Left-down	478 ± 40	347 ± 24
Middle-left-down		1293 ± 91
Middle-right-down		1765 ± 124
Right-down	1265 ± 15	916 ± 64
Chest	255 ± 16	

Table 2
Dose in fluorapatite dental ceramic samples. The position of teeth start in left-behind part (sample 1), samples 3–5 are in front of teeth and sample 8 is in right-behind part.

Sample ID	OSL measurement [mGy]	TL measurement [mGy]
1	230	232
2	242	229
3	306	280
4	315	301
5	283	281
6	205	239
7	317	308
8	237	231

that the photon energy dependence of the different materials is not expected to lead to a strong deviation between the absorbed dose in the material and the absorbed dose in air. Indeed, when using the dose per particle and energy interval information for glass and air plotted in Fig. 10 d for seat position 48, one can calculate a theoretically expected ratio of dose in glass to dose in air for this location of 1.25. Since the overresponse of resistor substrates and the encapsulation in chip cards have been shown in preliminary investigations to be in the same range or less than that of glass (Ekendahl and Judas, 2012; Beerten and Vanhavere, 2010), one can expect the dose in the former two materials to be also less than 30% higher than the dose in air. This is compatible with the experimental observation of the absorbed dose in BeO and Al_2O_3 reference detectors (Fig. 5 d). Moreover, this also means that the doses to the different materials for the same seat position will differ by much less than 25%, since the difference in energy response between the materials (e.g. resistor substrate and glass) is much less than the difference in energy response between glass and air. This implies that a comparison of doses to different components of personal items for the same seat position is reasonable.

A detailed map of the dose distribution can be qualitatively compared to the measured doses of the EPDs using the Monte Carlo simulation. In Fig. 11 the seating configuration and the EPD readouts are shown for the stronger source (1.5 TBq). The mapping of the dose was colored for illustration and can be compared to the dose distribution result for the simulation. The results fit very well and shielding of the water canister can be recognized in the visualization of the output data.

In conclusion the Monte Carlo calculations reflect the experimental results and are a useful radiation protection tool to estimate the dose distribution and energy spectra in a complex irradiation scenario.

3.6. Multi-method approach for dose estimation

The evaluation of the different dose assessment methods was so far carried out by comparison of the measured doses with individual, material specific reference dosimeters. In a real accident, reference doses are not available and outliers more difficult to identify. Combining the results of several dose assessment methods for the same personal item or individual could potentially help to increase the accuracy and robustness of retrospective dosimetry in general and reduce the number of outliers. Such an approach will be explored in this section.

In the two panels of Fig. 12 the comparison of the dose measurements using two independent components (display glass and resistors) of the same device as a function of seat number is shown, together with the results of the respective reference dosimeters and the simulated glass dose. For Fig. 12 b, the dose date from arbitrary chip cards with individual fading correction are additionally included. These data are a combination of the data shown in Fig. 6 a-b, 8 a-b, 9 d and 10 but by using the seat number as the common reference, the direct comparisons of the different assays is facilitated. As could be already seen from Fig. 5 a, the two reference dosimeters give similar answers as to the actually absorbed dose, with the dose in the LUXEL detectors being somewhat systematically lower than the dose in the reference glass, due to

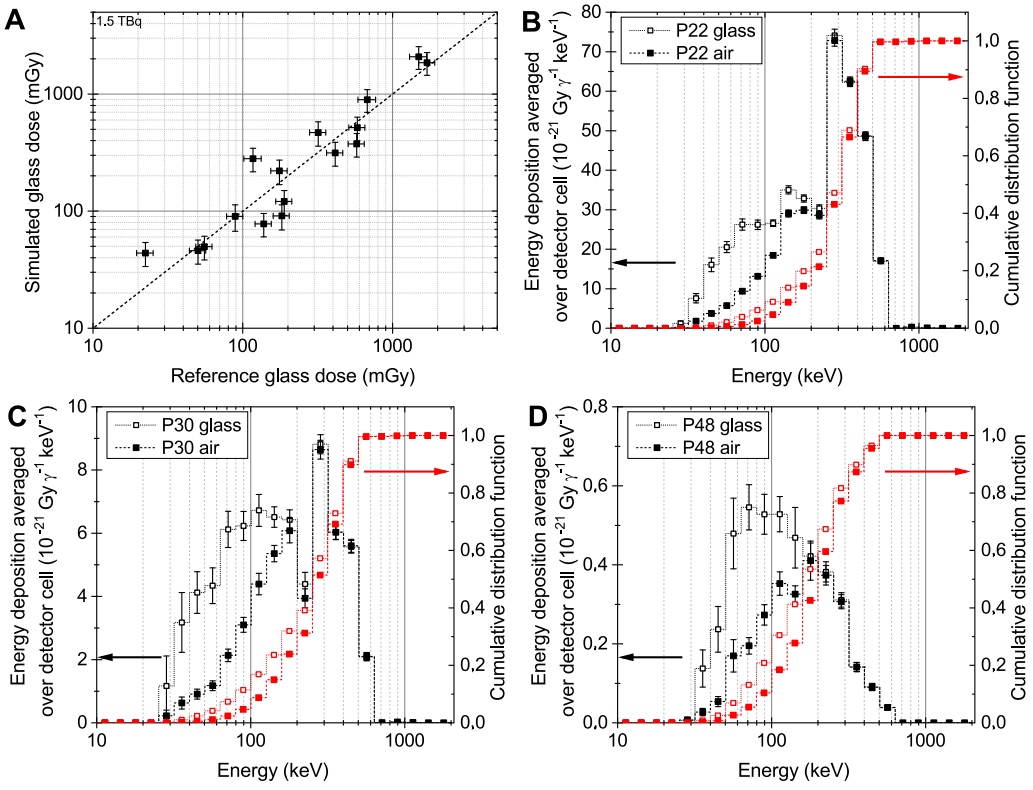

Fig. 10. A: Comparison of the simulated absorbed dose in glass, using Monte Carlo calculations, with the measured absorbed dose in reference glass for the exposure day with the stronger source (1.5 TBq). B–D: Photon energy spectra at different detector positions calculated from MCNP (in the form of dose per source particle per energy interval).

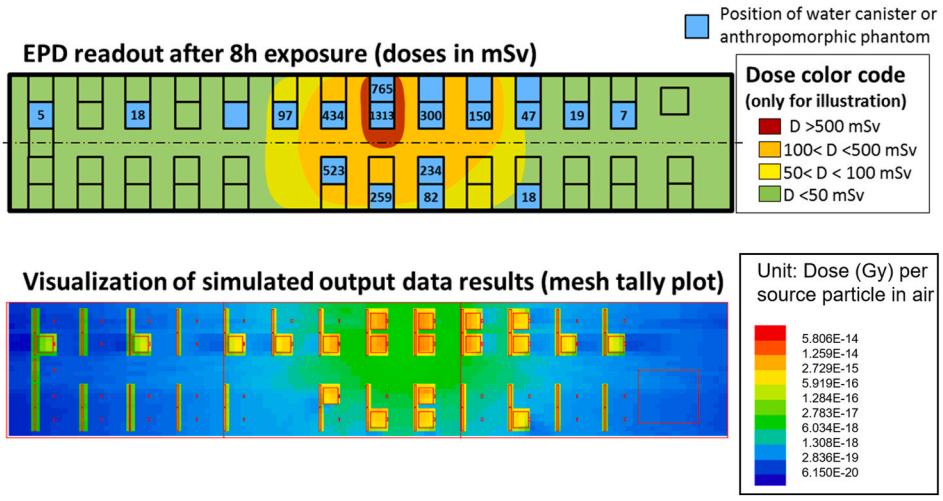

Fig. 11. Results of Monte Carlo calculations of the dose distribution in the bus for the stronger source (1.5 TBq).

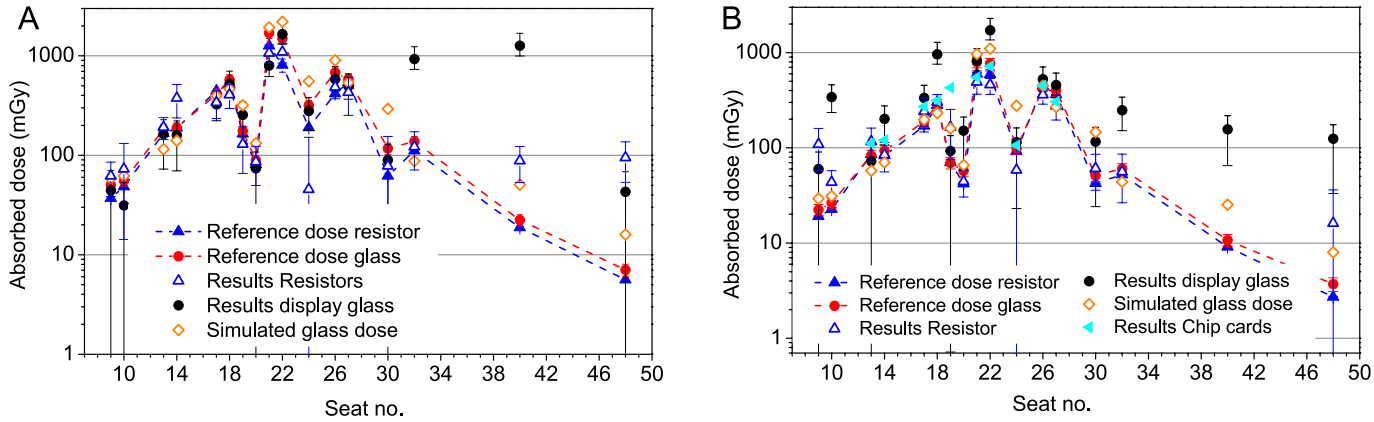

Fig. 12. a–b: Comparison of dose assessment using both components of the same mobile phone, display glass and resistor substrates, and simulation results for the exposure day using the 1.5 TBq (A) and 0.65 TBq source (B). For the latter the results of the dose measurement with the arbitrary chip cards with individual fading correction are additionally shown.

absorption by the phone itself. What is more interesting to see in both panels of Fig. 12 that most of the strong overestimations of the dose in display glass can be readily identified when combined with the dose information of the other assays. This can be clearly seen for e.g. seat numbers 32 and 40 in Fig. 12 a and seat numbers 10, 18, 22 and 32 in Fig. 12 b. For the most distant seat positions in Fig. 12 b (40 and 48) this might not be as obvious at first but can be reconstructed from the simulation results and known layout of the exposure geometry that require a decrease in dose when going from seat number 32 to 40, instead of an increase that would result if the combination of glass and resistor dose for seat number 32 (as the glass dose here was already marked as an outlier) and glass doses for the higher seat positions would be used. Additional support comes from the resistor doses for seat positions 40 and 48, which both were below detection limit (for seat number 40 this could not be plotted in Fig. 12 b as the dose was negative) but from which upper limits of 16 and 36 mGy could be inferred, which support the simulation results. Conversely the overestimation of the resistors doses for seat position 48 in Fig. 12 a and seat position 9 in Fig. 12 b can be identified in a similar fashion, by combining measured and simulated glass doses with the comparison with doses at other seat numbers and the expected decrease of doses with increasing distance from the source.

When using each dose assessment method by itself, a total of 13 outliers occurred for glass display and resistor doses. With the multi-method approach in the described fashion it was possible to reduce this number to three. A combination of at least three dose assays was necessary in the present case, the chip card doses were not explicitly used for this approach but strengthened the results of the other assays whenever they agreed (the apparent chip card dose outlier for seat number 19 in Fig. 12 b will be discussed further below). When combining only two dose assessment methods, e.g. resistor and glass doses, outliers might not be always readily identifiable but the strong discrepancy of the two dose results would stimulate a closer analysis and lead either to an identification of the true outlier, by the methods described e.g. in section 3.2.2 or at least to a significant reduction in the degree of over- or underestimation by averaging of the two dose measurement results. Such a multi-method approach will consequently significantly increase the accuracy and robustness of the dose assessment method using personal objects.

The apparent overestimation in the chip card dose for seat number 19 in Fig. 12 b requires closer inspection. For the other seat positions, chip cards and mobile phones were placed close to each other, for seat number 19 however, they were almost on opposite sides of the water canister. As indicated by the doses measured in the personal dosimeters on the water canister (Fig. 13), for this almost left-lateral exposure there was a strong gradient in doses of almost an order of magnitude from the left to the right side of the canister. Measured dose in the arbitrary chip card (No. 11) was (430 ± 40) mGy, reference dose on the adjacent chip card module 270 mGy, measured doses in the phone between 100 and 160 mGy. It thus seems that the electronic components in both mobile

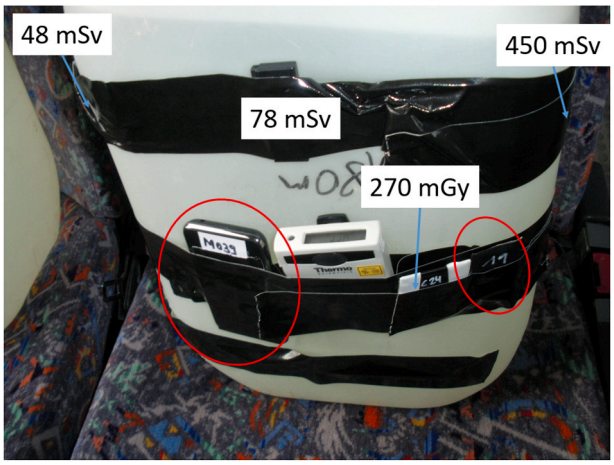

Fig. 13. Water canister on seat position 19 before irradiation with the 0.65 TBq source. The positions of the mobile phone and the chip card are marked with red circles. Additionally, the doses measured by OSL personal dosimeters at three positions of the canister (taken from Rojas-Palmas et al. (2020)) and in the LUXEL detector on the chip card module form Infineon, placed in between the (arbitrary) chip card and mobile phone, are given. (For interpretation of the references to color in this figure legend, the reader is referred to the Web version of this article.)

phone and chip card had recorded the respective local doses correctly within uncertainties but that the latter are not comparable but reflect the heterogeneity of the exposure. This can thus be seen as a first example that the measurement of doses in several personal items carried at different positions by the exposed individual can potentially be used not only to reconstruct doses but also exposure conditions. A second example is the phantom on seat number 22 for irradiation with the 1.5 TBq source, for which the combination of measured doses in the phone (1.1–1.5 Gy) and dental ceramics (0.23–0.31 Gy) clearly resolves a heterogeneous exposure along the height of the torso.

4. Conclusions

The proof-of-concept clearly helped to validate recently emerged dose reconstruction techniques in a realistic accident scenario. For each combination of material and measurement protocol tested the strengths and weaknesses can be summarized as follows:

- For resistors the strengths are a comparatively high sensitivity (detection limit of 50–70 mGy for measurments 10–20 days after exposure, when sampling 20 medium sized resistors; a lower detection limit is expected with newer generation OSL readers with higher LED stimulation power), the fact that the material has homogeneous dosimetric properties (fading rate), that standardized protocols for fast readout are applicable and that a low number of outliers occurred (only for doses below 100 mGy and then with a deviation of less than 100 mGy). The main weakness, being entirely non-scientific but relevant, is that currently sampling is not possible without destruction of the entire phone. This implies high replacement costs and a potential low acceptability of the method by the general population. Moreover, in modern smartphones it is difficult to find even 10 resistors of the preferred 0402 size. This means that either an increase of the detection limit has to be accepted or resistors of smaller size have to be sampled as well, which can be tedious and time consuming. Research into the use of other detection windows using TL that promise higher sensitivity should be explored (Lee et al., 2017).
- Inductors showed the highest sensitivity of all materials investigated (detection limit of 20 mGy (OSL) for measurements 36 days after exposure) and allowed dose assessment with low fading rate ($\leq$ 20%) when using TL. The weaknesses for this material are that not all smartphones contain these kind of inductors, that the fading rate in OSL is heterogeneous and that a consistent dose overestimation in TL was observed, which is not yet understood.
- For display glass there is generally a large amount of sample material available per phone, the display can be replaced at lower costs than the whole phone, a homogeneous fading rate was observed (with one exception) and the sensitivity was in an acceptable range (detection limit in the order of 100 mGy for etched glass, 15 days after exposure). On the other hand, high intrinsic background doses can occur, which can lead to dose overestimations up to 1 Gy. Some of these outliers can be identified by an internal analysis but not all.
- Chip cards are an item of low replacement costs with quick and easy sample preparation (minutes) and acceptable sensitivity (detection limits depending on chip size between 40 and 100 mGy for 20 days after irradiation), making them in principle very attractive for emergency dosimetry. However, in the field test here, a heterogeneous fading rate was found, which makes an individual post-accident assessment of the degree of fading necessary, otherwise larger uncertainties up to a factor of two have to be accepted.
- Monte Carlo simulations of radiation transport can give valuable additional information on expected doses, on photon spectra and can be used to convert dose in the material to dose in organs (Discher et al. in prep.). The main weaknesses of this method are that simulations are only as good as the information that go into them (i.e. a good knowledge of the exposure conditions is required), that it is not applicable to highly dynamic exposures and that complex geometries can take time to be implement in the code and then to be computed.

As the results of the field test demonstrated, none of the methods is completely fail-save. In 43 out of 61 cases, agreement between reference doses and doses measured by the radiation sensitive components of the mobile phones was observed within error limits, but in 13 cases outliers with a significant dose overestimation were observed. Some of these outliers were in the order of 100 mGy or less and might not have had a serious impact in a real accident, but they constituted a systematic deviation from the true (local) dose, nonetheless. The key was here to combine the dose results of several personal items and/or several radiation sensitive components of one item with Monte Carlo simulations. In this way, 10 of the 13 outliers could be identified. Generally, no dosimetry method was (yet) able to reconstruct doses below 50 mGy, either due to insufficient sensitivity or issues with possible pre-existing non-radiation induced signals.

Compared to a controlled laboratory irradiation, the field test was characterized by a possible higher uncertainty in reference dosimetry, contribution of scattered, lower energy photons, and variability in local doses by difference in positioning of different items on the water canisters. As could be shown, the use of dosimeters of similar composition as the radiation sensitive components of the personal item and placed as close as possible to the latter worked reasonably well to obtain accurate reference dose values. The impact of scattered radiation was found to lead to an increase of the absorbed dose in the different materials compared to dose to air by a maximum of 20–30%; much less difference could be expected when comparing doses in different materials directly. The dose difference in personal items in different positions on the canister was seen to be potentially useful to reconstruct exposure geometries. Such an approach could be more systematically investigated in future field experiments. The field test thus evaluated the potential and limitation of retrospective dosimetry using personal items and demonstrated the importance of using a multi-dosimeter approach to increase robustness of the method.

Declaration of competing interest

The authors declare that they have no known competing financial interests or personal relationships that could have appeared to influence

the work reported in this paper.

Acknowledgements

The research leading to these results has received funding from the European Community's Seventh Framework Program (FP7/2007–2013) under grant agreement n° 261693. We are grateful to the Austrian Army and the entire CATO field team for fantastic on-site support. We thank two anonymous reviewers for constructive criticism that helped to improve the quality of the manuscript.

Appendix A

Laboratory tests of the rapid screening protocol for chip cards

Previous to the field test, the time optimization of the measurement protocol for chip cards was examined in lab irradiation experiments using the same wire-bond chip card modules from Infineon as were used in the field test. Irradiations were performed by built-in beta source of the Risø TL/OSL DA-15 reader. Simulated accident doses between 90 mGy and 10 Gy were applied and read out using a single calibration dose point of 1 Gy without any test dose normalization. Two set of modules were used, one measured immediately after irradiation and the second one 6 days after irradiation. For the second set of modules the samples were then re-measured some time later, using an extended protocol with 300 s readout time, test dose normalization, four regeneration doses, a zero dose and lowest dose recycling point, similar to the protocol described in Woda and Spöttl (2009). A second dose was then calculated using the initial 30 s OSL measurement and the extended calibration curve. Results are shown in Fig. 14 a.

For measurements promptly after irradiation, the accuracy obtained with the rapid protocol is not as good as when applying an extended protocol, such as in Fig. 8 of Woda and Spöttl (2009). However, the results are still acceptable: for doses up to approx. 1 Gy, the measured dose is within 10% of the applied dose. For higher doses there is a systematic decrease in the measured dose, but even for 10 Gy the underestimation is still only 25%. This would be fully acceptable as a first screening result. The underestimation is possibly due to thermal transfer at room temperature from the 100 °C TL trap into the trap(s) responsible for the fast OSL components, as a result of the short OSL stimulation time (Woda and Spöttl, 2009), leading to a too high calibration dose signal and thus to a somewhat too low inferred dose. This effect will be more pronounced for higher accident-calibration dose ratios, as observed.

For the measurement six days after irradiation, the performance of the rapid protocol is somewhat poorer, but still acceptable (Fig. 14 b). For 90 mGy the measured dose is 75% of the given dose, for 200 mGy to 1 Gy around 80% and for higher doses the ratio systematically increases from 80% up to 120% (10 Gy). The subsequent application of the extended protocol leads to a significant improvement in accuracy for doses up to approx. 3 Gy but also to an increase in the overestimation for higher doses (40% for 10 Gy). Obviously, similar to Fig. 8 in Woda and Spöttl (2009), a systematic effect/error of the fading correction reverses the otherwise expected decrease of the measured dose with the rapid protocol for higher doses. This systematic effect might be that the fading correction curve is no longer even approximately dose independent for doses higher than 3–4 Gy and that as a consequence, the applied fading correction factor in Fig. 14 b is somewhat too high in this dose range. This was not an issue for the field test, since the highest dose occurred were below 2 Gy.

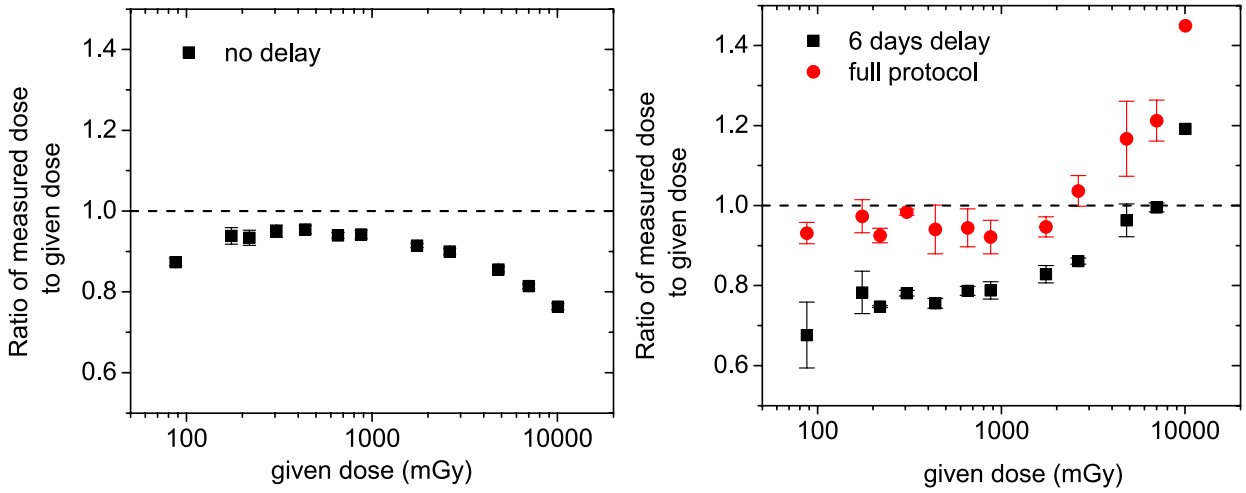

Fig. 14 a-b. Test of a time optimized protocol for rapid dose assessment with chip cards. The upper panel (A) shows the results of dose measurements immediately after irradiation, the lower panel (B) results for dose measurement six days after irradiation, with fading correction. The red, circle symbols denote the later measurement of the same modules using a full, extended protocol. Three to six modules were measured per dose point and the average and standard deviation plotted.

Appendix B. Supplementary data

Supplementary data to this article can be found online at https://doi.org/10.1016/j.radmeas.2021.106544.

References

Ademola, J.A., Woda, C., Bortolin, E., 2017. Thermoluminescence investigations on tobacco dust as an emergency dosimeter. Radiat. Meas. 106, 443–449.

Bailiff, I.K., Sholom, S., McKeever, S.W.S., 2016. Retrospective and emergency dosimetry in response to radiological incidents and nuclear mass-casualty events: a review. Radiat. Meas. 94, 83–139.

Bassinet, C., Le Bris, W., 2020. TL investigation of glasses from mobile phone screen protectors for radiation accident dosimetry. Radiat. Meas. 136, 106384.

Bassinet, C., Pirault, N., Baumann, M., Clairand, I., 2014a. Radiation accident dosimetry: TL properties of mobile phone screen glass. Radiat. Meas. 71, 461–465.
Bassinet, C., Woda, C., Bortolin, E., Della Monaca, S., Fattibene, P., Quattrini, M.C., Bulanek, B., Ekendahl, D., Burbidge, C.I., Cauwels, V., Kouroukla, E., Geber-Bergstrand, T., Mrozik, A., Marczewska, B., Bilski, P., Sholom, S., McKeever, S.W.S., Smith, R.W., Veronese, I., Galli, A., Panzeri, L., Martini, M., 2014b. Retrospective radiation dosimetry using OSL of electronic components: results of an inter-laboratory comparison. Radiat. Meas. 71, 475–479.
Bassinet, C., Kreutzer, S., Mercier, N., Clairand, I., 2017. Violet stimulated luminescence signal from electronic components for radiation accident dosimetry. Radiat. Meas. 106, 431–435.
Beerten, K., Vanhavere, F., 2010. Photon energy dependence of three fortuitous dosimeters from personal electronic devices, measured by optically stimulated luminescence. Radiat. Protect. Dosim. 140, 294–299.
Bortolin, E., Boniglia, C., Della Monaca, S., Gargiulo, R., Fattibene, P., 2011. Silicates collected from personal objects as a potential fortuitous dosimeter in radiological emergency. Radiat. Meas. 46, 967–970.
Browne, E., 2003. NM - CEA/LNHB - table de Radionucléides. Laboratoire National Henri Becquerel.
Currie, L.A., 2004. Detection and quantification limits: basic concepts, international harmonization, and outstanding ("low-level") issues. Appl. Radiat. Isot. 61, 145–149.
Discher, M., Woda, C., 2013. Thermoluminescence of glass display from mobile phones for retrospective and accident dosimetry. Radiat. Meas. 53–54, 12–21.
Discher, M., Eakins, J., Woda, C., Tanner, R., in prep. Translation of the Absorbed Dose in the Mobile Phone to Organ Doses of an ICRP Voxel Phantom Using MCNPX Simulation of an Ir-192 Point Source.
Discher, M., Woda, C., Fiedler, I., 2013. Improvement of dose determination using glass display of mobile phones for accident dosimetry. Radiat. Meas. 56, 240–243.
Discher, M., Hiller, M., Woda, C., 2015. MCNP simulations of a glass display used in a mobile phone as an accident dosimeter. Radiat. Meas. 75, 21–28.
Discher, M., Bortolin, E., Woda, C., 2016. Investigations of touchscreen glasses from mobile phones for retrospective and accident dosimetry. Radiat. Meas. 89, 44–51.
Discher, M., Woda, C., Lee, J., Kim, H., Chung, K., Lang, A., 2020. PTTL characteristics of glass samples from mobile phones. Radiat. Meas. 132, 106261.
Ekendahl, D., Judas, L., 2011. NaCl as a retrospective and accident dosemeter. Radiat. Protect. Dosim. 145, 36–44.
Ekendahl, D., Judas, L., 2012. Retrospective dosimetry with alumina substrate from electronic components. Radiat. Protect. Dosim. 150, 134–141.
Ekendahl, D., Judas, L., 2017. OSL and TL retrospective dosimetry with leucite glass-based dental ceramics. Radiat. Meas. 104, 1–7.
Ekendahl, D., Judas, L., Sukupova, L., 2013. OSL and TL retrospective dosimetry with a fluorapatite glass-ceramic used for dental restorations. Radiat. Meas. 58, 138–144.
Ekendahl, D., Bulánek, B., Judas, L., 2016. A low-cost personal dosemeter based on optically stimulated luminescence (OSL) of common household salt (NaCl). Radiat. Meas. 85, 93–98.
Fattibene, P., Trompier, F., Wieser, A., Brai, M., Ciesielski, B., De Angelis, C., Della Monaca, S., Garcia, T., Gustafsson, H., Hole, E. O., Juniewicz, M., Krefft, K., Longo, A., Leveque, P.,Lund, E., Marrale, M., Michalec, B., Mierzwinska, G., Rao, J. L., Romanyukha, A. A., Tuner, H. EPR dosimetry intercomparison using smart phone touch screen glass. Radiat. Environ. Biophys. 53, 311-320.
Fiedler, I., Woda, C., 2011. Thermoluminescence of chip inductors from mobile phones for retrospective and accident dosimetry. Radiat. Meas. 46, 1862–1865.
Gasparian, P.B.R., Vanhavere, F., Yukihara, E.G., 2012. Evaluating the influence of experimental conditions on the photon energy response of Al2O3:C optically stimulated luminescence detectors. Radiat. Meas. 47, 243–249.
Hubbell, J.H., Seltzer, S.M., 2004. Tables of X-Ray Mass Attenuation Coefficients and Mass Energy-Absorption Coefficients from 1 keV to 20 MeV for Elements Z = 1 to 92 and 48 Additional Substances of Dosimetric Interest. National Institute of Standards and Technology, Gaithesburg, MD, USA. https://doi.org/10.18434/T4D01F [Online].
IAEA - International Atomic Energy Agency, 2004. The Radiological Accident in Cochabamba. IAEA, Vienna.
ICRP – International Commission on Radiological Protection, 1997. Publication 74. Conversion coefficients for use in radiological protection against external radiation. Ann. ICRP 26 (3/4).
ICRU – International Commission on Radiation Units and Measurements, 2019. Methods for Initial-Phase Assessment of Individual Doses following Acute Exposures to Ionizing Radiation. ICRU Report 94.
Kim, H., Kim, M.C., Lee, J., Chang, I., Lee, S.K., Kim, J.-L., 2019. Thermoluminescence of AMOLED substrate glasses in recent mobile phones for retrospective dosimetry. Radiat. Meas. 122, 53–56.
Kim, H., Kim, M.C., Lee, J., Discher, M., Woda, C., Lim, S., Chang, I., Lee, S.K., Kim, J.-L., Chung, K., 2020. Characterization of thermoluminescence of chip cards for emergency dosimetry. Radiat. Meas. 134, 106321.
Lee, J.I., Kim, H., Kim, J.L., Pradhan, A.S., Kim, M.C., Chang, I., Lee, S.K., Kim, B.H., Park, C.Y., Chung, K.S., 2017. Thermoluminescence of chip inductors and resistors in new generation mobile phones for retrospective accident dosimetry. Radiat. Meas. 105, 26–32.
McKeever, S.W.S., Minniti, R., Sholom, S., 2017. Photo transferred thermoluminescence (PTTL) dosimetry using Gorilla ® glass from mobile phones. Radiat. Meas. 106, 423–430.
McKeever, S.W.S., Sholom, S., Chandler, J.R., 2019. A comparative study of EPR and TL signals in Gorilla(R) glass. Radiat. Protect. Dosim. 186, 65–69.
MCNPX-Team, 2003. MCNP - A General Monte Carlo N-Particle Transport Code, Version 5, Volume II: User's Guide. Los Alamos National Laboratory Report LA-CP-03-0245.
Mrozik, A., Kulig, D., Marczewska, B., Bilski, P., 2017a. Dose estimation based on OSL signal from banknotes in accident dosimetry. Radiat. Meas. 101, 1–6.
Mrozik, A., Marczewska, B., Bilski, P., Książek, M., 2017b. OSL signal of IC chips from mobile phones for dose assessment in accidental dosimetry. Radiat. Meas. 98, 1–9.
Rojas-Palma, C., Woda, C., Discher, M., Steinhäusler, F., 2020. On the use of retrospective dosimetry to assist in the radiological triage of mass casualties exposed to ionizing radiation. J. Radiol. Prot. 40, 1286. https://doi.org/10.1088/1361-6498/abc181.
Sholom, S., McKeever, S.W.S., 2014. Emergency OSL dosimetry with commonplace materials. Radiat. Meas. 61, 33–51.
Sholom, S., McKeever, S.W., 2016. Integrated circuits from mobile phones as possible emergency OSL/TL dosimeters. Radiat. Protect. Dosim. 170, 398–401.
Sholom, S., McKeever, S.W.S., Chandler, J.R., 2020. OSL dosimetry with protective glasses of modern smartphones: a fiber-optic, non-destructive approach. Radiat. Meas. 136, 106382.
Sommer, M., Freudenberg, R., Henniger, J., 2007. New aspects of a BeO-based optically stimulated luminescence dosimeter. Radiat. Meas. 42, 617–620.
Ulanowski, A., Hiller, M., Woda, C., 2021. Absorbed doses in bricks and TL-dosimeters due to anthropogenic and natural environmental radiation sources. Radiat. Meas. 140, 106458.
Williams, R.G., Gesh, C.J., Pagh, R.T., 2006. Compendium of Material Composition Data for Radiation Transport Modeling. PNNL-15870.
Woda, C., Spöttl, T., 2009. On the use of OSL of wire-bond chip card modules for retrospective and accident dosimetry. Radiat. Meas. 44, 548–553.
Woda, C., Discher, M., Rojas-Palma, C., Lettner, H., Kulka, U., Oestreicher, U., Della Monaca, S., Fattibene, P., Bassinet, C., Gregoire, E., Roy, L., Bulanek, B., Burbidge, C., Monteiro Gil, O., Van Hoey, O., Koroukla, E., Smith, R.W., Moquet, J., Geber-Bergstrand, T., Mrozik, A., Sholom, S., McKeever, S.W.S., Veronese, I., Vral, A., in preparation. Retrospective Dosimetry Using OSL of Electronic Components and Biological Dosimetry in a Realistic Accident Scenario: Results of an Inter-comparison.
Woda, C., Bassinet, C., Trompier, F., Bortolin, E., Della Monaca, S., Fattibene, P., 2009. Radiation-induced damage analysed by luminescence methods in retrospective dosimetry and emergency response. Ann. Ist. Super Sanita 45, 297–306.
Woda, C., Fiedler, I., Spöttl, T., 2012a. On the use of OSL of chip card modules with molding for retrospective and accident dosimetry. Radiat. Meas. 47, 1068–1073.
Woda, C., Kaiser, J.C., Urso, L., Greiter, M., 2012b. An environmental BeO-OSL dosimeter for emergency response. Radiat. Meas. 47, 609–613.
Zankl, M., 1999. Personal dose equivalent for photons and its variation with dosemeter position. Health Phys. 76, 162–170.